Industrial Bioresource Engineering
https://ojs.wiserpub.com/index.php/IBE/

Research Article

Optimization of Continuous Granular Flow in a Helical Screw-Induced Rotation Fluidized Bed Reactor: Cold Test Insights on Multi-Parameter Control

Arash Javanmard[1,2*], Fathiah Mohamed Zuki[1,2], Wan Mohd Ashri Wan Daud[1,2], Muhamad Fazly Abdul Patah[1,2*]

[1]Department of Chemical Engineering, University Malaya, 50603, Kuala Lumpur, Malaysia.
[2]Sustainable Process Engineering Centre (SPEC), Department of Chemical Engineering, Faculty of Engineering, University Malaya, Kuala Lumpur, Malaysia
E-mail: fazly.abdulpatah@um.edu.my

Received: 4 March 2025; **Revised:** 24 April 2025; **Accepted:** 28 May 2025

Abstract: This study investigates the Residence Time Distribution (RTD) behavior in a Helical Screw Reactor (HSR) by analyzing key performance indicators, including Mean Residence Time (MRT), average outlet flow rate (Ave_{out}), and Reynolds number (N_{Re}). Using a structured Design of Experiments (DOE) approach integrated with Response Surface Methodology (RSM), the influence of Feed Rate Speed (FRS) and Helical Screw Rotation Speed (HSRS) on reactor behavior was statistically examined. Results reveal that FRS has a significant effect on Ave_{out} ($F = 873.24$, $p < 0.0001$), whereas HSRS shows negligible influence ($p = 0.3673$). Interaction effects (FRS × HSRS) were statistically insignificant ($p = 0.5966$). A notable quadratic effect was observed for FRS ($F = 9.67$, $p = 0.0171$), indicating nonlinearity in its influence on Ave_{out}. The MRT model was statistically significant ($F = 4.55$, $p = 0.0363$), confirming that the selected factors sufficiently explain MRT variability. N_{Re} was strongly impacted by experimental parameters ($F = 132.66$, $p < 0.0001$), highlighting their critical role in reactor hydrodynamics. Perturbation plots demonstrated MRT and N_{Re} high sensitivity to FRS variations compared to HSRS. Model validation through diagnostic plots (normal Q-Q and residuals vs. factors) confirmed good model fit and random error distribution. These findings underscore the capability to fine-tune HSR reactor performance by optimizing FRS and HSRS, thereby enhancing mass transfer, mixing efficiency, and biomass feed consistency in thermochemical applications. This predictive modeling approach offers a valuable optimization framework for advancing continuous biomass conversion systems and improving the sustainability and efficiency of energy processes.

***Keywords*:** residence time distribution, design of experiments, response surface methodology, mass transfer rate, reynolds number

Nomenclature

Ave_{out}	Average outlet
DOE	Design of Experiments
FRS	Feeder Speed Rate

Copyright ©2025 Arash Javanmard, et al.
DOI:
This is an open-access article distributed under a CC BY license
(Creative Commons Attribution 4.0 International License)
https://creativecommons.org/licenses/by/4.0/

HSRS	Helical Screw Rotation Speed
HSIR	Helical Screw Rotation-Induced Fluidized Bed Reactor
MRT	Mean Residence Time
RTD	Residence Time Distribution
RSM	Response Surface Methodology
N_{Re}	Reynolds Number
ANOVA	The Analysis of Variance

1. Introduction

As civilizations advance, the demand for fuel rises. Because of the restrictions and disadvantages associated with fossil fuel sources, switching to renewable energy sources has become critical. This shift focuses on waste management and sustainable energy alternatives (Javanmard et al., 2024; Ofélia de Queiroz et al., 2024). This process not only taps into abundant and renewable resources but also aligns with global efforts to transition towards cleaner energy systems. Biomass is a critical element in the evolution toward a more sustainable and environmentally friendly energy landscape due to its ability to efficiently reduce pollution, greenhouse gas emissions, and energy security (Adeniyi et al., 2024). However, converting biomass to usable fuels requires advanced technologies, including biological and thermochemical processes (Javanmard et al., 2024; Javanmard et al., 2025). Despite their comparatively low capital costs and ease of operation, anaerobic digestion and composting are not preferred due to incomplete carbon conversion and prolonged residence times (Vaithyanathan et al., 2023). In contrast, thermochemical processes facilitate complete carbon conversion within a short residence time and high efficiency (Siwal et al., 2022).

However, the direct utilization of biomass in thermochemical processes faces several challenges, including high moisture content, low Oxygen-to-Carbon (O/C) ratio, low Fixed Carbon (FC), low Calorific Value (CV), poor grindability, and hydrophobicity (Javanmard et al., 2025; Javanmard et al., 2023; Lewandowski et al., 2020). Thermochemical conversion processes, including pyrolysis and gasification, play pivotal roles in this transformation by breaking down biomass into valuable energy products (Wang et al., 2022). Various systems have been designed for conducting thermochemical treatments, such as screw conveyors, drum reactors, vertical moving beds, fluidized beds, cyclonic reactors, and microwave reactors (Alauddin et al., 2010; Chen et al., 2023; Cremers et al., 2015; Moser et al., 2023).

Each system has unique operational characteristics and limitations. For example, fluidized or moving bed systems offer precise control over temperature and residence time but suffer from limited heat transfer and clogging, and are highly sensitive to particle size (Khodaei et al., 2015; Stegehake et al., 2019). Larger particles can hinder heat transfer, complicate mechanical feeding, and disrupt fluidization. Conversely, smaller particles can lead to issues such as particle entrainment, uneven residence times, and variability in the treatment's final severity for each particle (Cai et al., 2021; Motta et al., 2018). Rotary kilns, cylindrical vessels that rotate and provide uniform heating, are energy-intensive, require complex maintenance, and offer limited flexibility for different feedstocks (Alonso et al., 2017; Qureshi et al., 2020). These challenges underscore the need to optimize reactor designs and operational parameters to improve efficiency and product quality. Table 1 presents a comparison of common thermochemical reactor technologies.

Table 1. Comparison of common thermochemical reactor technologies

Reactor Type	Advantages	Disadvantages	Working conditions	Ref
Rotary Drum	Demonstrated, low-pressure drops, direct and indirect heating	Low heat rate, difficult temperatur control, large, difficult to scale	Moderate to high temperatures	(Soponpongpipat et al., 2020)
Screw Conveyor	Can handle larger particles, Plug flow possible, proven technology	Uneven heat distribution, potential for incomplete conversion, difficult to scale	Moderate to high temperatures	(Nachenius et al., 2015; Ünsaç et al., 2024)
Multiple Hearth	Demonstrated, good scale up, easy control	Low heat rate, limited capacity, large	Moderate to high temperatures	(Lacombe et al., 2024)
Vertical Moving Bed	Efficient heat transfer, simple operation	High pressure drops, difficult temperature control, difficult to handle for particle sizes	High temperatures, requires uniform feedstock	(Korba et al., 2022)
Belt Conveyor	Demonstrated, easy scale up, low pressure drops, high heating rate	Difficult to handle varying particle sizes, complexity, difficult temp control	High temperatures	(Infiesta et al., 2019)
Fluidized Bed	High heat rate, scalable, uniform temperature distribution	Requires precise control of particle size, fluidizing gas needed,	Consistent fluidization airflow, High temperatures	(Hanchate et al., 2021; Soria-Verdugo et al., 2023)
Microwave Reactor	Fast heating rates, Selective heating capabilities	Limited penetration depth, high equipment costs	Moderate to high temperatures, requires microwave energy source	(Goyal et al., 2022)

Given these challenges, optimizing the reactor design and operational parameters is essential to enhance the efficiency and output quality of thermochemical conversion processes. The HSIR has emerged as a promising technology owing to its potential for continuous processing and efficient heat transfer (Abdulyekeen et al., 2024; Abdulyekeen et al., 2022). However, optimizing the operation of HSIR fluidized bed reactors presents a significant challenge due to the complex internal flow behavior and mixing dynamics. A core element in understanding this behavior is RTD analysis, which reveals how particles travel within the reactor, directly influencing mixing efficiency, reaction kinetics, and overall process performance. Despite their promising potential in biomass conversion systems, fundamental research on HSIR reactors remains scarce, especially regarding the dynamics of continuous granular flow. This knowledge gap served as the primary motivation for the present study.

This research is the first to systematically investigate and optimize the dynamic behavior of an HSIR reactor using cold test-based RTD analysis, combined with Design of Experiments (DOE) and Response Surface Methodology (RSM). The experimental study evaluates how two critical operational parameters, Feeder Rotation Speed (FRS) and Helical Screw Rotation Speed (HSRS), affect key performance indicators: Mean Residence Time (MRT), Average outlet flow rate (Ave_{out}), and Reynolds Number (N_{Re}), a proxy for mixing intensity. The novelty of this work lies in its integrated multi-parameter optimization framework, which enables precise control of continuous flow conditions in a helical screw-driven fluidized bed reactor. By quantifying and modeling the impact of FRS and HSRS on flow behavior, this study delivers first-of-its-kind baseline data for reactor-scale prediction and design. These insights pave the way for improved reactor configurations and operational strategies, offering a transformative approach to continuous biomass processing. Ultimately, the outcomes support more efficient, controllable, and sustainable thermochemical conversion technologies, pushing the frontier of energy systems research.

2. Materials and methods

2.1 *Tracer preparation*

Figure 1 shows the preparation process for Palm Kernel Shell (PKS), which was sourced from the Palm Oil Mill, Sime Darby Berhad, Malaysia, and used as the primary material for granular flow (tracer). Initially, the PKS was air-dried under the sun for 72 hours to reduce surface moisture. The dried material was ground to obtain particles with a 1-2 mm size range, ensuring uniformity for subsequent treatments. The ground PKS was placed in an oven and heated at 378 K for 24 hours to eliminate any residual moisture content that could interfere with later processes.



Figure 1. Process flow chart

2.2 *Reactor design*

Figure 2 shows the experimental setup and design characteristics of the HSRI reactor. The reactor was constructed from stainless steel, featuring a thickness of 5 mm, an internal diameter of 228 mm, and a total length of 1,524 mm. The stainless steel helical screw used in this study measured 1,550 mm in length, with 6 flights, a pitch distance of 95.25 mm, and an external diameter of 203.2 mm (Qureshi et al., 2021). To regulate the continuous feeding of the tracer into the reactor, an auger-based feeding system driven by an AC motor was utilized. The operational range for FRS was set between 10 and 100 rpm, corresponding to the functional limits of the motor and the flow requirements of the system (Figure 2). Similarly, the HSRS was also varied within the 10-100 rpm range. These intervals were selected based on the mechanical and design specifications of the reactor components, ensuring stable material transport, efficient mixing, and alignment with the reactor's intended processing capacity (Qureshi et al., 2021). The chosen ranges reflect practical operating conditions that are both achievable and safe within the current system configuration. They were specifically tailored to capture the dynamic behavior of the reactor under realistic cold test conditions, while enabling a comprehensive analysis of how FRS and HSRS influence residence time distribution and flow characteristics.

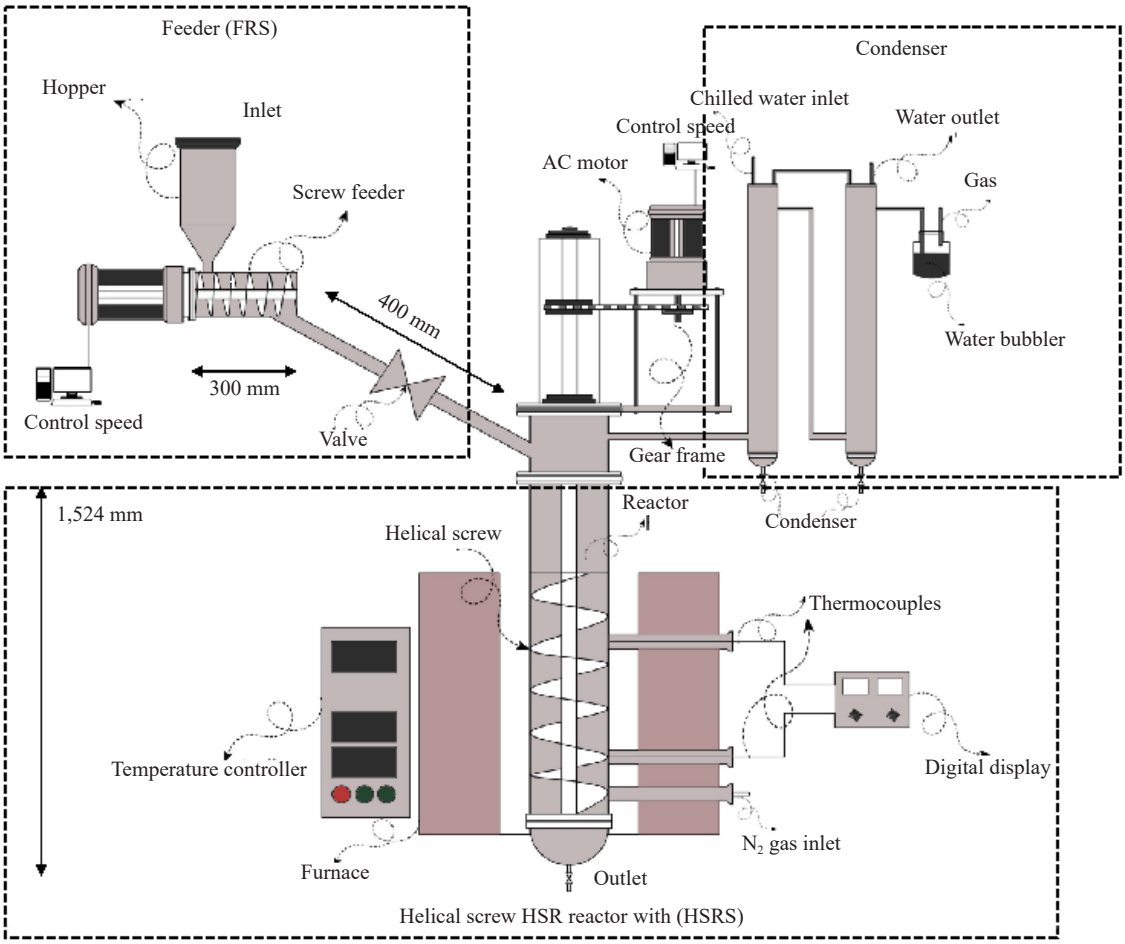


Figure 2. Helical screw rotation-induced fluidized bed reactor (HSR) setup

2.3 *Experimental design matrix*

The conventional method for optimizing multi-parameter-dependent processes has limitations due to its One-Factor-at-A-Time (OFAT) approach, which neglects the interactive effects among independent variables (Huter & Strube, 2019). The Response Surface Methodology (RSM) is suggested as a statistically effective method to optimize multi-factor processes by considering the interactive effects of independent variables (Veza et al., 2023). This study used Design Expert Version 13.0.5 software (State-Ease Inc., USA) to design the experiment, model development, regression analysis, and optimization. We employed a two-factor Face Central Composite Design (FCCD) of RSM to determine the optimum conditions and analyze the main, interactive, and quadratic effects of the independent variables (HSRS and FRS) on three dependent variables: The Mean Residence Time (MRT), mass transfer (Ave_{out}), and Reynolds Number (N_{Re}). Figure 3 shows the flowchart of the experimental process design. Moreover, this investigation's design matrix, randomly generated with 13 experimental runs and three responses (MRT, Ave_{out}, and N_{Re}), is presented in Table 2.

Table 2. Levels of independent variables in the design matrix

Factor		Level and range			Std.dev
Code	Name (unit)	-1	0	+1	
A	Helical Screw Rotation Speed (rpm)	10	60	100	32.66
B	Feeder rotation speed (rpm)	10	60	100	32.66

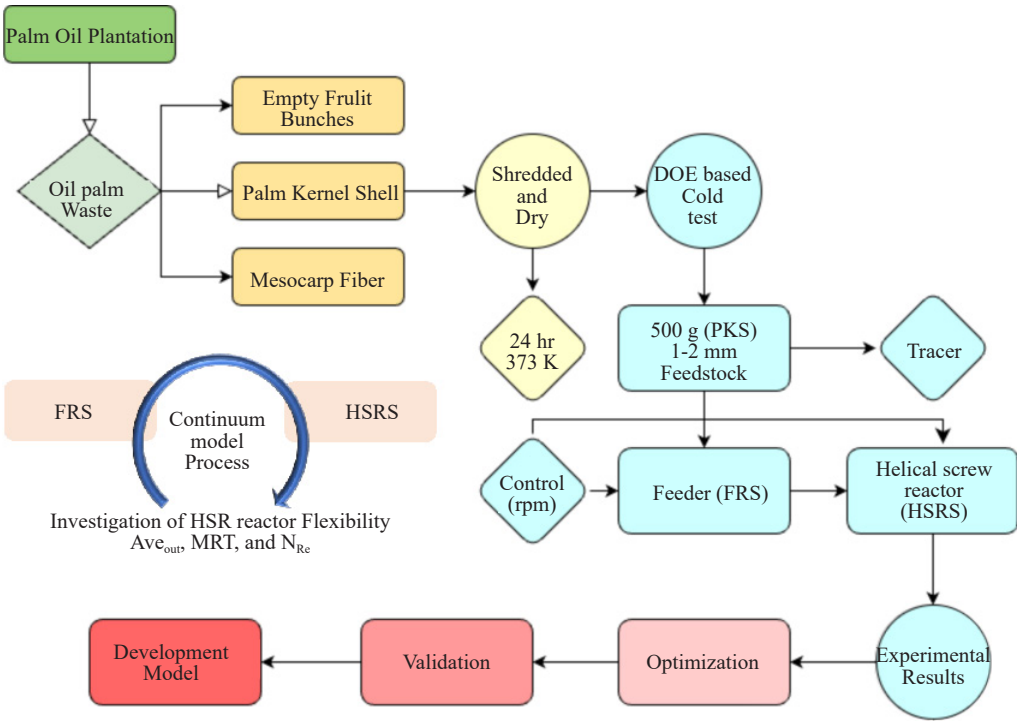


Figure 3. Optimization process design flow chart

2.4 *Experimental methodology*

To create the granular flow within the HSIR reactor at room temperature and pressure, we employed 500 g of PKS with particle sizes ranging from 1-2 mm as a tracer in each experimental session. The purpose of the tests was to methodically examine the impacts of two crucial operating parameters: HSRS and FRS.

The tracer particles were fed into the reactor while varying both the FRS and HSRS to analyze the resulting changes in flow dynamics. To ensure a steady state throughout the experiments, all valves were kept open, and the outlet weight was continuously monitored. MRT, Ave_{out}, and N_{Re} were the primary performance indicators measured in response to these speed variations. The helical screw, acting as the mechanical mixing agent, was observed under different conditions to capture its behavior and role in enhancing the flow, distribution, and transport of particles (Qureshi et al., 2021). Each test captured how changes in FRS and HSRS influenced the granular flow and the performance of the reactor, focusing on optimizing the continuous flow of particles. Data were collected and analyzed to provide insights into how FRS and HSRS individually and jointly affect MRT and mixing efficiency, critical parameters for the system's operational efficiency and performance. This methodical approach allowed for a comprehensive understanding of the dynamic relationships between FRS, HSRS, and key process variables, laying the groundwork for optimizing the reactor for continuous biomass conversion processes (Veza et al., 2023).

The RSM was employed to develop predictive models for each of the responses (MRT, mass transfer, and mixing efficiency). This statistical approach allowed us to generate quadratic equations for each response based on the experimental data. These models were then validated by comparing the experimental results with the predicted outcomes derived from the RSM. The accuracy of these models was crucial for the optimization phase (Alsarraf et al., 2025).

By capturing the behavior of the helical screw as a mechanical mixing agent under different FRS and HSRS settings, we systematically analyzed the impact of these variables on reactor performance. Each test demonstrated how changes in FRS and HSRS affected the granular flow, residence time, and mixing efficiency. The final step involved optimizing the system using the generated models and comparing the results with experimental data to validate the efficacy of the optimization process. This integrated approach provided deep insights into the dynamic interactions between the operational parameters, leading to recommendations for optimizing the continuous flow of particles and enhancing the reactor's overall performance for biomass conversion processes. The reproducibility of data and experimental error were evaluated using five repeated center points, resulting in a standard error of less than 3%.

2.5 *Methods of calculation of dependent factors*

The Residence Time Distribution (RTD) is a vital parameter for comprehending how fluids behave within reactors. It offers valuable insights into how tracer fluids are distributed over time, shedding light on various flow behaviors such as stagnation, channeling, or plug flow (Bhalode et al., 2021). The distribution function $E(t)$, representing the duration of the tracer fluid in the reactor, provides a thorough understanding of fluid flow patterns and mean residence time. By scrutinizing these curves, we can grasp the overall fluid flow behavior in the vessel and optimize operational efficiency accordingly (Rodrigues, 2021). Equation (1) represent the $E(t)$:

$$E(t) = \frac{QC(t)}{N_0} = \frac{C(t)}{\int_0^\infty C(t)dt} = \frac{2}{\sigma\sqrt{\pi}} \exp - \left[\frac{\left(t - t^-\right)^2}{\sigma^2} \right]. \quad (1)$$

Where Q represents the volumetric flow rate, $C(t)$ denotes the concentration of the mass flow rate, N signifies the moles of tracer injected into the reactor (here the amount of mass considered $g \cdot min^{-1}$), t represents the mean residence time, and σ^2 indicates the variance. The denominator represents the integral of the C-curve, and $E(t)$ denotes the probability that a mass entering the reactor at $t = 0$ exits the reactor at time t.

$$\int_0^\infty E(t)dt = 1 \quad (2)$$

The RTD curve mirrors the E-curve, wherein the area beneath the curve at any time denote's the percentage mass that has left the reactor up to that point (Ding et al., 2022). This similarity is seen in the RTD curve, where the area under the curve at any moment represents the proportion of mass that has exited the reactor until that instant. By integrating the E-curve, we obtain the cumulative distribution function, $F(t)$, also known as the F-curve, indicating the fraction of mass that has exited the reactor by a particular time.

$$F(t) = \int_0^t E(t)dt \quad (3)$$

Plotting the curves helps detect irregularities in the system, like double peaks, asymmetrical distributions, or extended tails. These anomalies can be quantified, and the mixing performance is assessed using the first, second, and third moments (Cherkasov et al., 2023). The first moment, which is the mean residence time, signifies the average duration fluid elements remain within the system, which is extracted from RTD data by using the following Equation:

$$MRT = \int_0^\infty t \cdot E(t)dt$$

$$= \frac{\int_0^\infty tE(t)dt}{\int_0^\infty E(t)dt} = \frac{\int_0^\infty tCdt}{\int_0^\infty Cdt}$$

$$= \frac{\sum t_i C_i \Delta t_i}{\sum C_i \Delta t_i} \tag{4}$$

To elucidate the flow dynamics, we utilized a dimensionless parameter called the Reynolds Number.

$$N_{Re} = \frac{DV\rho}{\mu} = \frac{DV}{v} \tag{5}$$

The variables (D) signify the reactor's diameter, (V) the mass average velocity, (μ) the viscosity of the mass, as Kinematic viscosity, and (ρ) the density of the tracer. This study consists of analyzing the acquired experimental data through calculations utilizing software tools such as Microsoft Excel, Origin Pro, and MATLAB.

3. Results

This investigation thoroughly examined the RTD using F-curve analysis based on DOE runs, which is a sophisticated method for evaluating fluid dynamics within the system. The F-curve, a crucial tool in reactor analysis, delineates the temporal distribution of the tracer concentration, offering detailed insights into the flow dynamics within the reactor (Wojewódka et al., 2019). Figure 4 illustrates the F-curve of the system based on DOE runs, visually representing the dynamic tracer flow behaviors and the residence times within the reactor.

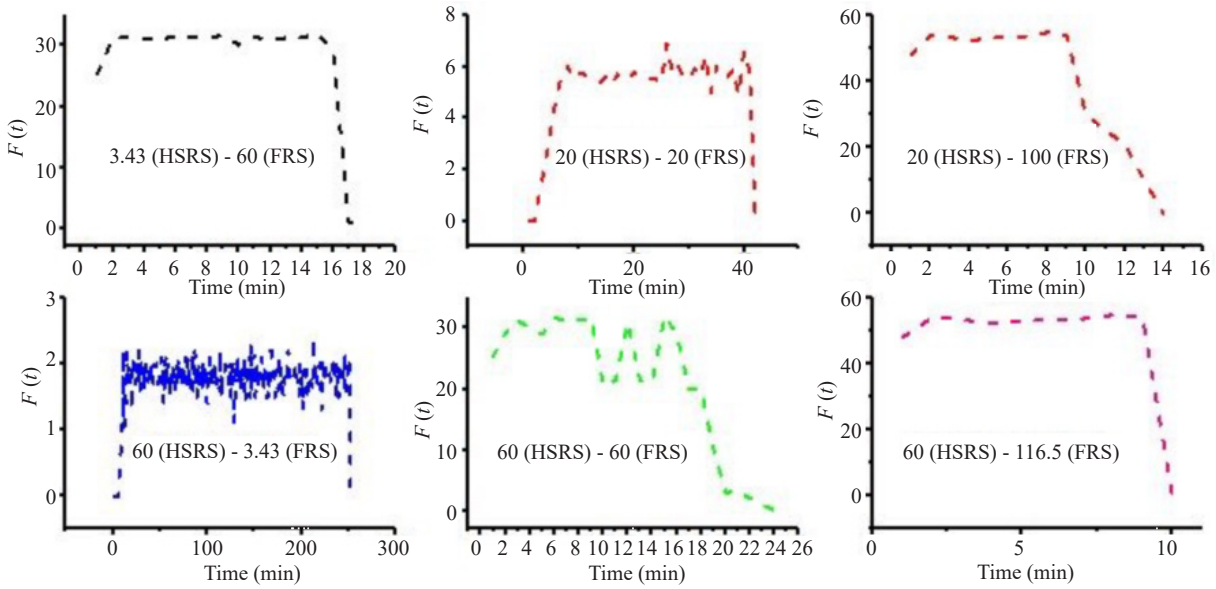


Figure 4. F-curve of different runs based on DOE

The detailed analysis revealed three distinct phases within the *F* curve: an ascending phase indicating the influx of fluid elements, depicted in Figure 4 as the first region influenced by varying FRS and HSRS; a steady-state region where the system reaches equilibrium; and a descending phase representing the efflux of fluid elements. As the FRS increased, a corresponding rise in the *F*-curve was observed, indicating higher tracer concentrations within the reactor. These results agree with theoretical expectations, as higher FRS naturally enhances the influx of fluid elements into the system. Consequently, a noticeable reduction in the duration of the steady-state region was observed, ned time frame for the system to achieve equilibrium due to the accelerated flow induced by increased FRS.

Furthermore, according to Equation (6), our comprehensive computational analyses demonstrated a concurrent decrease in the MRT, as precisely documented in Table 2. This empirical evidence supports the notion of expedited fluid element passage through the reactor, highlighting the significant impact of operational parameters on reactor kinetics.

3.1 *Influence of FRS and HSRS on flow characteristics: Trends in Ave_{out}, MRT, and N_{Re}*

The effects of FRS and HSRS on key flow parameters, MRT, Ave_{out}, and N_{Re}, were systematically analyzed through a set of 13 carefully designed experimental runs. The summarized data, presented in Table 3, reveal clear trends that underscore the dynamic influence of these two operational variables. A notable observation is that increasing the FRS consistently leads to higher Ave_{out} values, reflecting enhanced mass transport through the system. For instance, in runs where the FRS was set to its maximum of 100 rpm (runs 3 and 8), the average flow rate peaked at 46 g·min^{-1}, demonstrating the system's capacity for high-throughput feeding. In contrast, significantly lower FRS values, such as 3.43 rpm in run 11, resulted in a dramatic reduction of Ave_{out} to just 0.7 g·min^{-1}, illustrating the sensitivity of the outlet flow rate to feeder speed adjustments.

Table 3. FCCD experimental design matric with Ave_{out}, MRT, and N_{Re}

Run	HSRS (rpm)	FRS (rpm)	$(Ave_{Out})_{exp}$ (g/min)	$(Ave_{Out})_{pred}$ (g/min)	Residual	MRT_{exp} (min)	MRT_{pred} (min)	Residual	$(N_{Re})_{exp}$	$(N_{Re})_{pred}$ ($\times 10^3$)	Residual ($\times 10^3$)
1	60	60	28.97	28.97	0.0000	25	25.20	-0.2000	16×10^3	13.56	2.43
2	20	20	5.36	6.31	-0.9400	43.64	99.15	-55.51	2.19×10^3	5.03	-2.83
3	20	100	46	43.84	2.16	14	9.00	5.00	2.23×10^3	14.2	-12.01
4	3.43	60	25	25.65	-0.6521	30	2.39	27.61	17×10^3	8.01	8.9
5	60	60	28.97	28.97	0.0000	25	25.20	-0.2000	16×10^3	13.56	2.43
6	60	60	28.97	28.97	0.0000	25	25.20	-0.2000	16×10^3	13.56	2.43
7	100	20	7.3	8.47	-1.17	65	109.09	-44.09	13×10^3	12.87	0.120
8	100	100	46	44.06	1.94	10	6.42	3.58	20×10^3	22.09	-2.09
9	60	60	28.97	28.97	0.0000	25	25.20	-0.2000	16×10^3	13.56	2.43
10	60	116.5	48	50	-2.70	9	32.24	-23.24	12×10^3	20.08	1.9
11	60	3.43	0.7	-1.01	1.71	240	177.67	62.33	0.9×10^3	7.04	-6.1
12	116.5	60	27	27.34	-0.3397	10	1.48	8.52	19×10^3	19.1	-0.115
13	60	60	28.97	28.97	0.0000	26	25.20	0.8000	16×10^3	13.56	2.4

On the other hand, MRT showed an inverse relationship with both FRS and HSRS. Higher rotation speeds led to shorter residence times, due to the accelerated movement of materials through the reactor. For example, run 11, which had the lowest FRS, yielded the longest MRT at 240 minutes, suggesting prolonged retention and potentially more uniform processing. In contrast, run 8, where both FRS and HSRS were at their maximum (100 rpm), showed a sharply reduced MRT of just 10 minutes, reflecting rapid material turnover.

Additionally, both parameters significantly influenced the N_{Re}, which characterizes the flow regime. Higher FRS and HSRS values promoted more turbulent conditions, as seen in run 8, where N_{Re} reached 20×10^3, indicating vigorous mixing and enhanced momentum transfer. Conversely, run 11, operating at the lowest FRS, produced the lowest N_{Re}

value of 0.9×10^3, indicative of laminar flow and lower mixing intensity.

These findings demonstrate a delicate interplay between operational speed settings and flow dynamics. While increasing FRS and HSRS improves throughput and mixing (as indicated by higher Ave_{out} and N_{Re}), it concurrently reduces MRT, which may limit reaction time in thermochemical processes. Therefore, achieving optimal reactor performance requires a strategic balance: setting the FRS and HSRS to ensure sufficient material residence time while maintaining efficient flow and mixing. These insights form a critical foundation for future efforts to scale up and control HSIR systems for continuous biomass conversion processes.

3.2 *Statistical modeling and sensitivity analysis of reactor parameters using RSM*

The link between MRT, Ave_{out}, N_{Re}, FRS, and HSRS variables was investigated using response surface analysis. After thorough model development, the best fit for MRT, Ave_{out}, and N_{Re}, were achieved with quadratic models for the first two and a linear model for the last. These models, expressed in terms of coded factors, are summarized in Equations (7), (8), and (9), respectively.

$$Ave_{out} = -7.85 + 0.125HSRS + 0.62FRS - \left(0.3 \times 10^{-3}\right)(HSRS.FRS) - \left(0.7 \times 10^{-3}\right)HSRS^2 - \left(0.1 \times 10^{-2}\right)FRS^2 \quad (6)$$

$$\text{Mean Residence time} = 25.20 - 1.37HSRS - 51.42FRS - 6.34HSRS.FRS - 12.37HSRS^2 + 39.88FRS^2 \quad (7)$$

$$Re = 759.01 + 98.15HSRS + 4.6 \times 10^3 FRS \quad (8)$$

These equations serve as a valuable tool for predicting and offering insights into how these factors influence the factors within the system. The outcomes of the Analysis of Variance (ANOVA) test, which is used to evaluate the effectiveness of various models, are displayed in Tables 4, 5, and 6.

Analyzing model performance using ANOVA revealed some key insights. Analyzing model performance using ANOVA revealed some key insights.

The ANOVA for Ave_{out} presented in Table 4 provides significant insights into the factors influencing this response variable. The Ave_{out} analysis revealed several key insights. The HSRS factor, with a *p*-value of 0.3673 and an *F*-value of 0.3673, was not statistically significant at the 95% confidence level, indicating that variations in HSRS alone do not significantly impact the Ave_{out}. In contrast, the FRS was highly significant, with a *p*-value of < 0.0001 and an *F*-value of 873.24. This indicates that changes in FRS substantially affect the Ave_{out}, with higher FRS values correlating with increased outlet flow rates, aligning with the expectation that increasing feeder speed increases output rate.

The interaction term between HSRS and FRS (AB) has an *F*-value of 0.3074 and a *p*-value of 0.5966, indicating it is not significant. This suggests there is no significant combined effect of HSRS and FRS on the Ave_{out} beyond their individual effects. The quadratic term for HSRS (A^2), with a *p*-value of 0.1044 and an *F*-value of 3.48, is also not statistically significant, indicating that non-linear effects of HSRS are not important for the average outlet. However, the quadratic term for FRS (B^2) is significant, with a *p*-value of 0.0171 and an *F*-value of 9.67, indicating a quadratic relationship between FRS and the Ave_{out}. This non-linear effect means that after a certain point, increasing FRS will have a less-than-proportional effect on the Ave_{out}. Overall, FRS is the dominant factor influencing the average outlet flow rate, with a significant quadratic effect.

Table 4. ANOVA results for Ave_{out} model

Source	Sum of square	Df	Mean square	*F*-value	*p*-value
Model	2,713.00	5	542.60	177.26	< 0.0001[a]
A-HSRS	2.84	1	2.84	0.3673	0.3673
B-FRS	2,672.99	1	2,672.99	873.24	< 0.0001
AB	0.9409	1	0.9409	0.3074	0.5966
A^2	10.65	1	10.65	3.48	0.1044
B^2	29.59	1	29.59	9.67	0.0171
Residual	21.43	7	3.06		
Lack of Fit	21.43	3	7.14		
Pure Error	0.0000	4	0.0000		

Std. dev. = 1.75, mean = 26.94, C.V.% = 6.49, R^2 = 0.9922, R^2_{adj} = 0.9866, R^2_{pred} = 0.9443, Adeq precision =43.4973, a: significant

Table 5 presents the results of the ANOVA for MRT, which demonstrates a statistically significant impact of the model. The results were encouraging, indicating a statistically significant effect of the model (*F*-value = 4.55, *p*-value = 0.0363). This means that the factors included in the model collectively explain a significant portion of the variation in MRT, with a confidence level of 96.37% (1 *p*-value). In simpler terms, the model successfully captures the influence of these factors on the average length of an object residing within the system.

Table 5. ANOVA results for MRT model

Source	Sum of square	Df	Mean square	*F*-value	*p*-value
Model	34,572.08	5	6,914.42	4.55	0.0363[a]
A-HSRS	14.92	1	14.92	0.0.0098	0.9239
B-FRS	21,148.36	1	21,148.36	13.91	0.0074
AB	160.78	1	160.78	0.1058	0.7545
A^2	1,064.90	1	1,064.90	0.7006	0.4302
B^2	11,062.37	1	11,062.37	7.28	0.0307
Residual	10,640.40	7	1,520.06		
Lack of Fit	10,639.60	3	3,546.53	17,732.67	< 0.0001[a]
Pure Error	0.8000	4	0.2000		

Std. dev. = 38.99, mean = 42.13, C.V.% = 92.55, R^2 = 0.9647, R^2_{adj} = 0.9663, R^2_{pred} = 0.7345, Adeq precision = 6.9499, a: significant

Table 6 displays the ANOVA results for the N_{Re}, assessing the effectiveness of our linear regression model in capturing data variability. The results are promising, indicating a significant impact of the model (*F*-value = 132.66, *p*-value < 0.0001). This proves that the factors integrated into the model collectively elucidate a substantial portion of

the data's variance, effectively linking these factors to the observed variations in the dependent variable. However, it is important to recognize the presence of residual variation, indicating some unexplained aspects. This residual variance can stem from several factors. First, there might be additional variables influencing the dependent variable not accounted for in the model. Additionally, inherent random fluctuations are inevitable in any dataset. Finally, the linear regression model itself may have limitations in fully capturing the intricate relationship between variables. To address these potential limitations, future research could focus on identifying and integrating missing variables, exploring alternative model structures that better fit the data, or refining the existing model to achieve a more comprehensive understanding.

Table 6. ANOVA result for Reynolds Number (N_{Re}) model

Source	Sum of square	Df	Mean square	*F*-value	*p*-value
Model	2.933 + 08	2	1.467 + 08	4.75	0.0355[a]
A-HSRS	1.233 + 08	1	1.233 + 08	3.99	0.0736
B-FRS	1.700 + 08	1	1.700 + 08	5.51	0.0409
Residual	3.088 + 08	10	3.088 + 07		
Lack of Fit	3.088 + 08	6	5.147 + 07		
Pure Error	0.0000	4	0.0000		

Std. dev. = 5,557.07, mean = 13,563.08, C.V.% = 40.97, R^2 = 0.8714, R^2_{adj} = 0.8463, R^2_{pred} = 0.8112, Adeq precision = 6.3952, a: Significant

3.2.1 *Sensitivity assessment and model validation via perturbation analysis and ANOVA metrics*

The perturbation plot in ANOVA was used to assess the sensitivity of the response variable to changes in the predictor variables. In these plots, one predictor variable is varied while all other predictors are held constant at a reference point, typically their mean values. The response variable is then plotted against the varied predictor, resulting in a curve that shows the sensitivity of the response to that specific predictor (Sharma et al., 2019).

The perturbation plots presented in Figure 5 (a, b, and c) offer valuable visual insights into how the output responses, MRT, Ave_{out}, and N_{Re}, respond to variations in the operational parameters. The steep gradients observed in these plots, particularly along the FRS axis, indicate that FRS has a significantly greater influence on the reactor's flow behavior compared to HSRS. In other words, even small changes in FRS result in substantial shifts in MRT, Ave_{out}, and N_{Re}, highlighting its dominant role in controlling mass transfer, residence time, and flow regime within the reactor.

In support of these findings, the statistical analysis further reinforces the robustness and reliability of the developed models. The lack-of-fit *p*-values for MRT, Ave_{out}, and N_{Re} were found to be statistically insignificant, indicating no substantial discrepancy between the experimental data and the model's predictions. This confirms that the models provide a good fit and effectively capture the relationships between the variables under investigation.

Moreover, the models' sufficient precision values, 6.9499 for Ave_{out}, 6.3952 for N_{Re}, and 43.4973 for MRT, significantly surpass the generally recognized threshold of 4. These values reflect a strong signal-to-noise ratio, signifying that the models are capable of distinguishing meaningful variations in the design space. In practical terms, this means the models can confidently be used to predict outcomes, perform optimization, and guide operational adjustments in reactor settings.

Taken together, the perturbation plot analysis and statistical validation provide compelling evidence that FRS is the most critical controllable parameter in this system, playing a central role in determining reactor performance metrics. The reliability of the models, as affirmed by their statistical strength and predictive capability, makes them highly suitable for further applications in reactor scale-up, process control, and real-time optimization in continuous biomass processing systems.

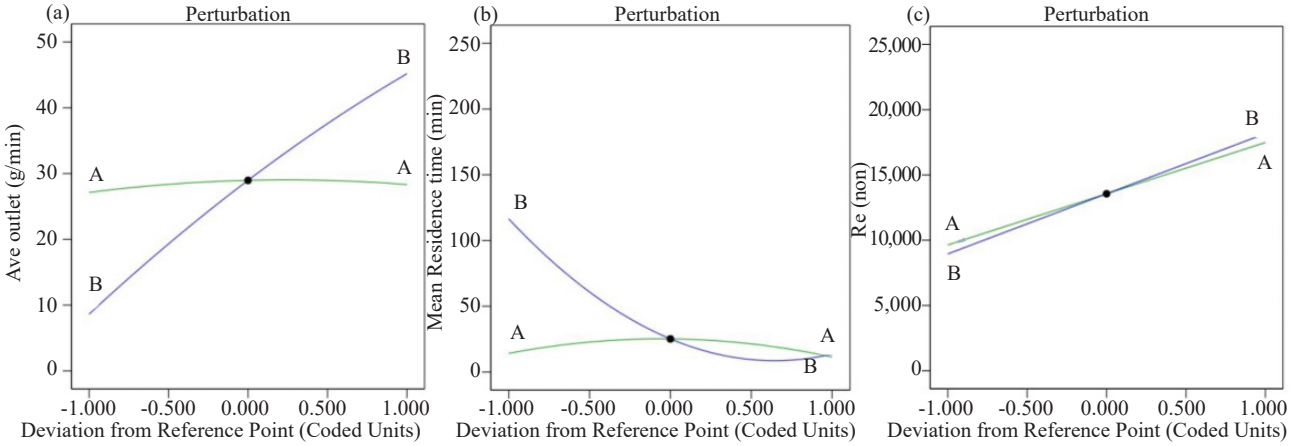


Figure 5. Perturbation plots of Ave_{out} (a), MRT (b), and N_{Re} (c)

3.2.2 *Comprehensive model diagnostics and interaction visualization*

Diagnostic plots were used to assess the model's accuracy and suitability further. The results are shown in Figures 6, 7, and 8. The probability plot of residuals (Q-Q plot) for Ave_{out} (a), MRT (b), and N_{Re} (c) is shown in Figure 6 under the assumption that their distributions are normal. The model's validity and dependability are supported by the observation that errors are distributed randomly and residuals are normally distributed. This increases confidence in the inferences made from the analysis by confirming that the model's assumptions are met. The robustness of the model's predictions and the reliability of conclusions drawn about the relationships between variables are guaranteed by the residual's normality.

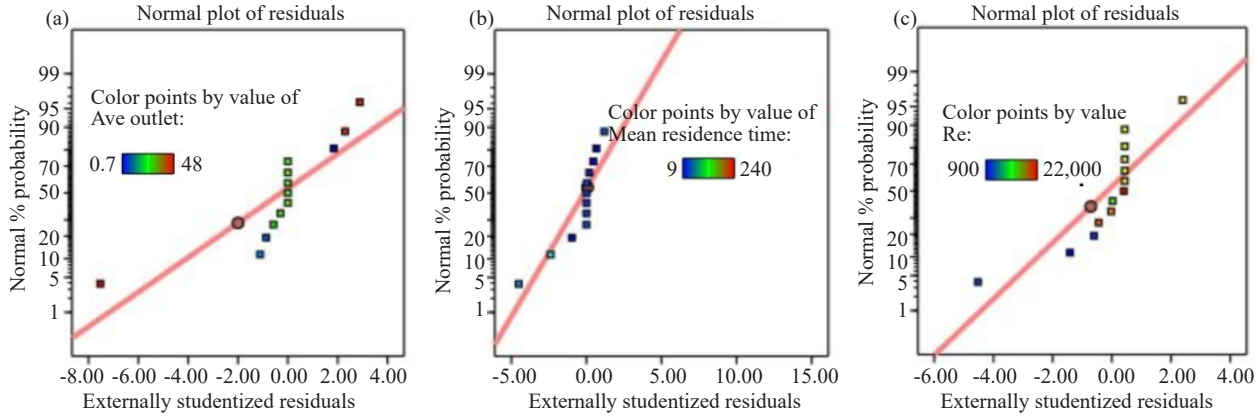


Figure 6. Normal plot of residual of Ave_{out} (a), MRT (b), and N_{Re} (c)

Figures 7 illustrate the comparison between actual and predicted values for Ave_{out} (a), MRT (b), and N_{Re} (c). The actual values were obtained from experimental measurements, and the predicted values were calculated using Equations (7), (8), and (9). The figures reveal a strong correlation between the predicted and experimental data, indicating that the models accurately reflect the relationship between the influencing factors and response variables. This strong relationship is supported by the high values of the model's correlation coefficients (R^2). Specifically, the adjusted R^2, (R^2_{adj}) values for MRT, Ave_{out}, and N_{Re} are 0.9866, 0.966, and 0.846, respectively, which are very close to their corresponding R^2 values of 0.9922, 0.8647, and 0.871. These close R^2 and R^2_{adj} values suggest that the models are reliable. Additionally, the predicted R^2 (R^2_{pred}) values aligned well with the R^2_{adj} values, with differences of less than

0.4. This alignment further implies that the model terms are significant across the design space, thereby confirming the robustness and predictive accuracy of the models. Overall, the high correlation coefficients and the alignment between R^2, R^2_{adj}, and R^2_{pred} values indicate that the models are significant and reliable for making predictions within the studied design space, meaning that they can be trusted to provide accurate predictions for MRT, Ave_{out}, and N_{Re} based on the given factors.

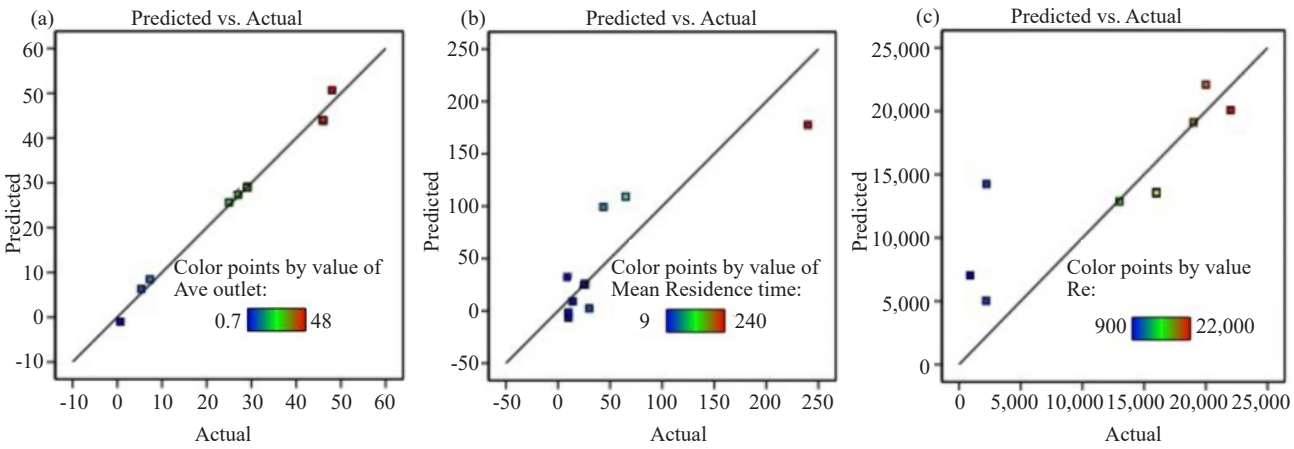


Figure 7. Predicted vs Actual plots of Ave_{out} (a), MRT (b), and N_{Re} (c)

Figures 8a, b, and c illustrate outlier plots for MRT, Ave_{out}, and N_{Re} across all experimental runs, respectively. The analysis examined how much each data point deviated from the expected value (residuals). Any residuals falling outside the shaded areas (red control limits in the figures) were considered outliers, meaning they differed significantly from the expected pattern. The standard deviation was used to define these control limits, with thresholds of ± 4.5611 and ± 3.86016. In all the data, only one point fell outside these limits, and interestingly, it corresponded to the experiment in which the FRS was set to either the highest or lowest value. This indicates that the models are consistent with the data within these limits, demonstrating their robustness and reliability across most experimental conditions. The presence of only one outlier suggests that aside from extreme FRS values, the models effectively capture the relationship between the predictors and the response variables.

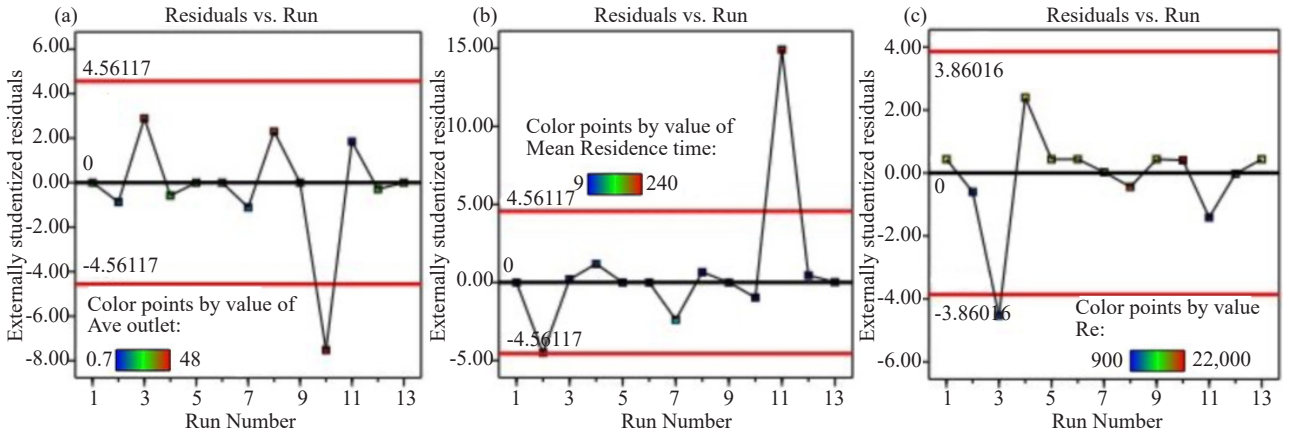


Figure 8. Residual vs run plots of Ave_{out} (a), MRT (b), and N_{Re} (c)

The randomly scattered residuals observed in the plot of studentized residuals versus predicted values for MRT, Ave_{out}, and N_{Re} in Figure 9 (a, b, and c) imply the models' goodness of fit. This random scatter indicates that there are no discernible patterns or trends in the residuals, which suggests that the models do not suffer from systematic bias. The randomness supports the validity of the models, confirming that the models accurately capture the underlying relationships between the predictors and the response variables and that the assumptions of the regression analysis are met. To further assess the validity of our regression models, we examined residual vs. factor plots for MRT, Ave_{out}, and N_{Re}, which are shown in Figures 10a, b, and c. Although the plots for Ave_{out} and MRT showed some scatter, a potential trend was observed in the N_{Re} residuals with increasing/decreasing values as FRS or HSRS increased. This suggests a possible violation of the homoscedasticity assumption in the N_{Re} model.

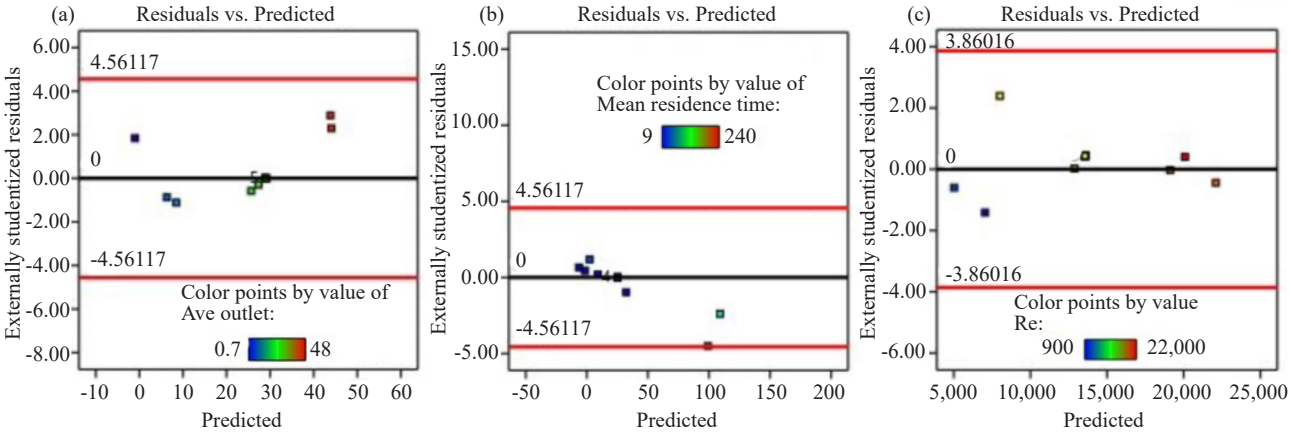


Figure 9. Residual vs predicted plots of Ave_{out} (a), MRT (b), and N_{Re} (c)

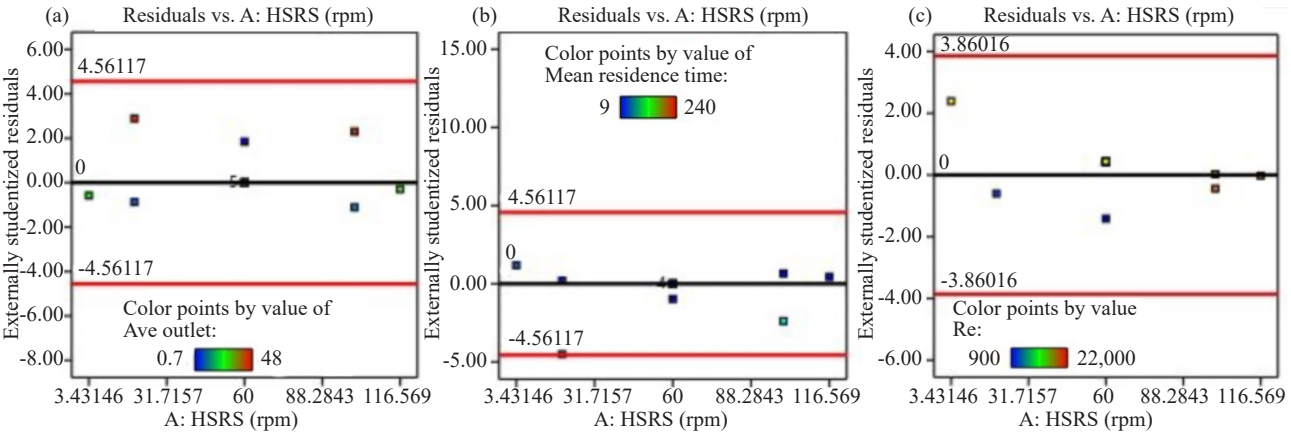


Figure 10. Residual vs factors plots of Ave_{out} (a), MRT (b), and N_{Re} (c)

To identify optimal settings for multiple dependent variables simultaneously, RSM utilizes contour plots to visualize the combined effects of independent variables on dependent variables. Figures 11a, b, and c show the contour plots of MRT, Ave_{out}, and N_{Re}, respectively. In this case, the RSM analysis yielded three distinct contour plots, each revealing a unique relationship between FRS, HSRS, and a specific dependent variable.

Figures 11a and b show the complex interactions between FRS and HSRS for Ave_{out} and MRT, respectively. The color intensity in these plots represents the magnitude of the dependent variable for different combinations of independent variables. Based on the color scale, darker colors likely represent higher Ave_{out} concentrations (Figure 11a), while lighter colors indicate lower concentrations. Examining the plot, the highest Ave_{out} values (darkest color) are

achieved at a combination of high FRS and high or intermediate HSRS. Conversely, lower Ave_{out} values (lighter color) are observed at a combination of low FRS and either high or low HSRS. This emphasizes the interaction effect, where the optimal FRS level for maximizing Ave_{out} depends on the HSRS level.

Similar to the Ave_{out} plot, the color scale indicates longer MRT (darker color) and shorter MRT (lighter color), as shown in Figure 11b. The plot suggests that longer MRT occurs at a combination of low FRS and high HSRS. On the other hand, shorter MRT is seen at high FRS and either low or high HSRS. Once more, the interaction effect is clear, since both the HSRS level and FRS have an impact on the intended MRT.

A significant observation in both plots is the absence of parallel straight contour lines. This suggests an interaction effect. In simpler terms, the influence of FRS on, for example, Ave_{out} is dependent on the HSRS level and vice versa. This highlights the need to consider both FRS and HSRS when optimizing dependent variables. The contour plot for the N_{Re} is shown in Figure 11c. The plot also reveals valuable information. The color scale suggests a range of N_{Re} values, with darker colors representing higher values and lighter colors indicating lower values. The observed curved contours confirm a more intricate relationship between the NRe, FRS, and HSRS compared to the other two plots. These findings are consistent with those of Qureshi et al. (2021).

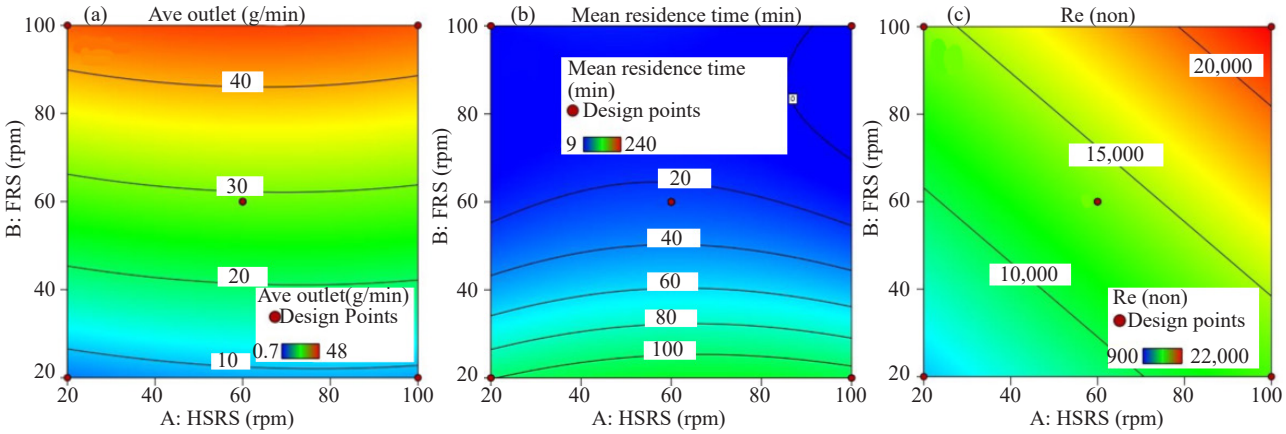


Figure 11. Contour plots of Ave_{out} (a), MRT (b), and N_{Re} (c)

3.3 *Optimization*

As discussed in Section 4.1, MRT, Ave_{out}, and N_{Re} reach their lowest and highest levels under specific circumstances. In this work, the responses (MRT, Ave_{out}, and N_{Re}) were optimized for several circumstances: (i) minimum (MRT, Ave_{out}, and N_{Re}) as low severity, obtained at (HSRS: 20 rpm, and FRS: 21.65 rpm) with desirability (0.756) (ii) maximum MRT, Ave_{out}, and N_{Re} as optimum severity, obtained at (HSRS: 98.98 rpm, FRS: 100 rpm) with desirability (0.972); and (iii) maximum MRT (high mean residence time) and minimum (Ave_{out}), and maximum N_{Re} as a moderate condition for comparison, obtained at (HSRS: 100 rpm, FRS: 20 rpm) with desirability (0.590), shown in Table 7. We selected these optimized conditions because increasing the HSRS enhances the mixing rate of biomass within the reactor, resulting in uniform heat distribution and mass transfer throughout the moving biomass. This observation aligns with the findings of Qureshi et al. (2019), which highlighted the superior performance of samples processed at higher HSRS. The optimized conditions, which are characterized by the lowest MRT, highest Ave_{out}, and highest N_{Re}, ensure efficient and consistent processing within the reactor.

Table 7. Predicted and experimental values of Ave_{out}, MRT, and N_{Re} at optimized conditions

Parameter	Low	Optimum	Optional
HSRS	20	98.98	100
FRS	21.65	100	20
Experimental (Ave_{out})	8.1	45.30	8.47
Predicted (Ave_{out})	7.24	44.119	9.1
Deviation	0.86	1.19	-0.63
Experimental MRT (min)	96	7	109.095
Predicted MRT	94.07	5.60	111
Deviation	1.93	1.4	-2
Experimental ($\times 10^3$)	4.5	23	12.87
Predicted ($\times 10^3$)	5.2	22	13.4
Deviation ($\times 10^3$)	-0.7	1	-0.53
Desirability	0.756	0.972	0.590

4. Discussion

4.1 *Process optimization using RSM and validation of predictive accuracy*

The optimization of the HSR reactor process was meticulously studied using RSM to determine the most effective operating conditions. The 3D and contour plots present the factors' (HSRS and FRS) interactive impacts on the responses (Ave_{out}, MRT, and N_{Re}), as displayed in Figure 12a-f. The key variables analyzed were the HSRS and FRS to optimize the Ave_{out}, MRT, and N_{Re}. Table 7 shows the predicted and experimental values of Ave_{out}, MRT, and N_{Re} at optimized conditions. One notable parameter is the HSRS, which has been significantly improved from its initial low value of 20 to an optimum of 98.98, approaching the maximum desirable setting of 100. This indicates that the RSM effectively identified settings that maximize the HSRS parameter, crucial for achieving optimal performance in high-speed rail systems. This combination was selected to provide balanced and efficient operation. Increasing the HSRS enhances the biomass mixing rate within the reactor, leading to a uniform heat distribution. This outcome is in line with the findings of Qureshi et al. (2019), who demonstrated that higher HSRS values improve the quality of samples due to better mixing dynamics.

Similarly, the FRS parameter shows substantial improvement, with an increase from 21.65 to 100 at the optimal setting of 20. This enhancement underscores the success of the optimization process in terms of enhancing system responsiveness under varying conditions. The experimental and predicted Ave_{out} values also improved significantly, transitioning from 8.1 to 45.30 experimentally and from 7.24 to 44.119 predicted, indicating a close alignment between experimental observations and model predictions. This close alignment indicates the robustness of the RSM model in accurately predicting the flow rate, which is essential for maintaining consistent reactor performance.

Deviation values, which measure the difference between experimental and predicted outcomes, generally decreased or remained stable, signifying improved predictive accuracy in the optimized settings. For instance, the MRT in minutes shows a notable reduction from an experimental value of 96 to 7 and a predicted value decrease from 94.07 to 5.60. This indicates that the optimized settings not only enhance the system performance but also align closely with theoretical predictions. The model's predictive power in terms of MRT is crucial, as it ensures that the biomass has sufficient time for conversion without excessive retention, which could lead to inefficiencies (Li, 2016).

Moreover, the N_{Re}, a critical parameter in fluid dynamics, demonstrated improvements in both experimental and predicted values. The experimental values increased from 4.5 to 23, while predicted values improved from 5.2 to 22, indicating better control and understanding of fluid dynamics within the system under study. These values suggest that

the models possess a sufficient signal-to-noise ratio, enabling them to effectively navigate the design space and make reliable predictions.

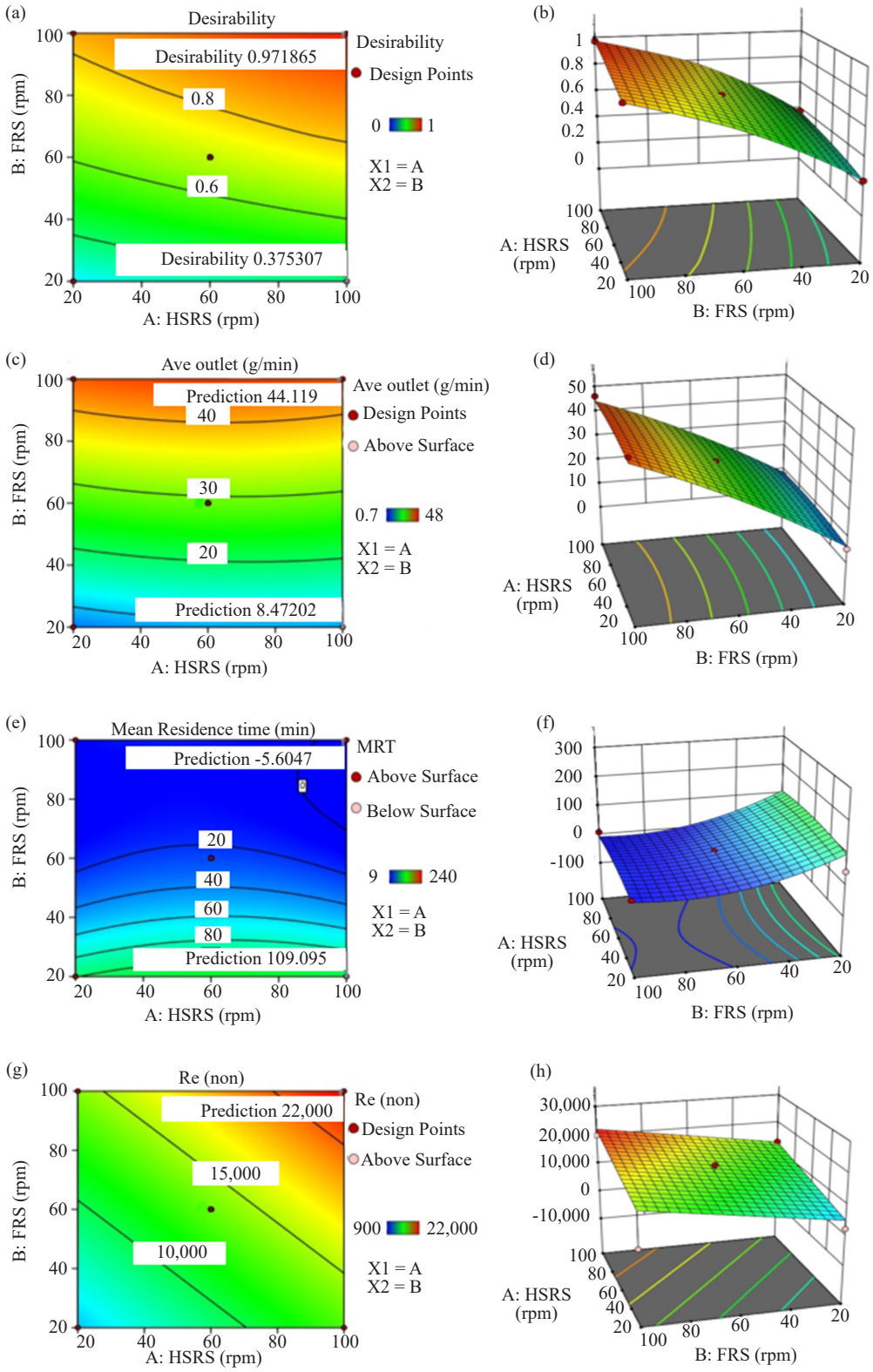


Figure 12. Contour and 3D surface plots for optimization condition, (a and b) desirability, (c and d) Ave_{out}, (e and f) MRT, and (g and h) N_{Re}

4.1.1 *Multi-objective optimization using desirability functions*

In multi-objective optimization, desirability functions serve as a powerful tool for balancing and harmonizing conflicting goals. These functions are typically constructed by applying mathematical transformations and weights to individual response variables, thereby converting each into a standardized scale ranging from 0 (completely undesirable outcome) to 1 (fully desirable outcome) (Harkare et al., 2024). This enables researchers to prioritize specific outcomes, such as maximizing throughput, minimizing residence time, or achieving optimal flow regimes, according to the objectives of the study (Seurin & Shirvan, 2024). For instance, in a reactor optimization context, maximizing average outlet flow (Ave_{out}) while simultaneously minimizing MRT and enhancing mixing efficiency (N_{Re}) reflects a set of competing goals (Wu et al., 2022). The desirability function unifies these criteria into a single scalar value that quantifies overall system performance under a given set of experimental conditions.

In the current study, RSM was employed to explore the design space and generate desirability contour plots, comparing performance at low, moderate, and optimum settings of the operational parameters. As shown in Figure 13, the optimized condition achieved a desirability value of 0.972, indicating a near-ideal configuration. This high desirability reflects simultaneous improvements across key performance indicators, including maximized Ave_{out}, minimized MRT, and enhanced N_{Re}, achieved by fine-tuning the FRS and HSRS. In contrast, the low and moderate conditions yielded significantly lower desirability values, with the lowest being 0.756, highlighting the suboptimal nature of those settings.

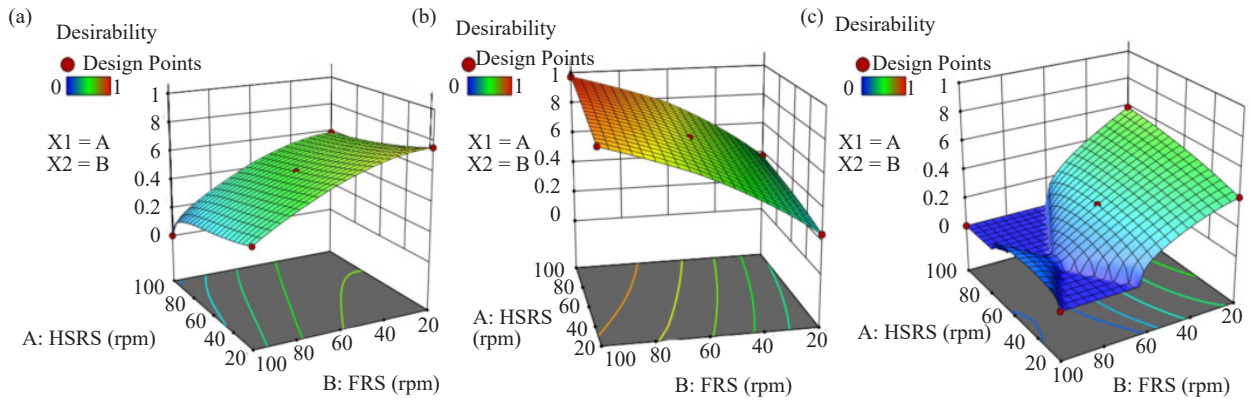


Figure 13. Desirability 3D surface plots for optimization conditions; (a) low, (b) optimum, and (c) moderate

Furthermore, the alignment between experimental and predicted results under optimal conditions confirms the robustness and predictive strength of the developed models (Sadrossadat et al., 2022). This outcome not only validates the effectiveness of the desirability function in navigating complex, multi-dimensional optimization challenges but also underscores the practical utility of RSM in enhancing the operational efficiency of novel reactor configurations, such as the HSIR fluidized bed reactor. RSM offers a structured, statistically robust approach for modeling and analyzing the relationships between multiple input variables and response outcomes (Reji & Kumar, 2022). Its strength lies in its ability to reduce the number of experimental trials needed while still delivering high-resolution insights into parameter interactions, making it particularly advantageous for systems where experiments are time-consuming or resource-intensive. Moreover, when combined with desirability functions, RSM enables the simultaneous optimization of multiple responses, balancing trade-offs such as residence time, flow behavior, and turbulence, to meet specific performance goals (Dianyu et al., 2024). However, RSM does have limitations: it assumes that system responses can be well-approximated by polynomial functions, which may not always capture highly nonlinear or chaotic behavior (Weremfo et al., 2023). Additionally, it may overlook subtle effects in regions not well-sampled during experimental design. Despite these drawbacks, the application of RSM in this study proves highly effective, offering predictive accuracy and operational clarity, and setting a precedent for its use in optimizing complex fluidized bed systems with helical screw-induced flow. To reinforce these findings, the perturbation plots and 3D response surface plots for the

optimized conditions are provided in the Supplementary Material, visually illustrating the responsiveness of key outputs to variations in the design variables.

Overall, the substantial increase in desirability, from 0.756 at suboptimal conditions to 0.972 at optimal conditions, demonstrates the success of the optimization strategy. It underscores the potential of data-driven modeling and design tools to guide the development of more efficient, scalable, and predictable processes in continuous biomass conversion and other thermochemical applications (Lambrinidis & Tsantili-Kakoulidou, 2021).

4.2 *Concluding remarks and practical implications*

When all is said and done, our study demonstrates the precise control that is achievable within an HSR reactor by manipulating the HSRS and FRS and systematically proves the flexibility of this reactor in controlling process-related factors. The close correlation between the experimental and predicted values of critical metrics based on RTD (Ave_{out}, MRT, and N_{Re}) demonstrates the robustness and reliability of the RSM model. This prediction accuracy is vital for optimizing the reactor's performance, ensuring efficient biomass conversion, and enhancing the overall system efficiency (Veza et al., 2023).

In detail, increasing the HSRS notably improves the mixing rate within the reactor. This mixing enhancement leads to a more uniform heat distribution across the biomass, ensuring that all particles are subjected to consistent processing conditions. Such uniformity is crucial for achieving consistent conversion rates and high-quality end products. On the other hand, the FRS directly affects the biomass feed rate into the reactor, thereby influencing the residence time and flow dynamics. An optimal FRS ensures a steady and controlled supply of biomass, mitigating issues such as clogging and irregular feed rates, which could otherwise disrupt the conversion process.

The findings of this study have broader implications, offering valuable insights that can be applied to other biomass conversion processes. The ability to predict and optimize reactor conditions is a powerful tool for researchers and engineers. By leveraging these insights, it is possible to develop more efficient and sustainable energy systems. These advances are particularly relevant in the context of increasing global emphasis on renewable energy sources and the need for environmentally friendly and efficient biomass conversion technologies.

4.3 *Statistical insights and RTD parameter sensitivity analysis*

In this study, we rigorously examined the factors affecting the RTD in an HSIR fluidized bed reactor, focusing on key parameters such as the MRT, Ave_{out}, and N_{Re}. Since thermochemical processes like pyrolysis, combustion, and torrefaction depend on an understanding of mass transfer and reactor mixing rate, these concepts are essential (Tumuluru et al., 2021). For the first time, we employed RSM to develop predictive models, thereby offering a novel and detailed framework for optimizing HSIR reactor operations.

The ANOVA results indicate that the HSRS does not significantly influence the Ave_{out}, with a *p*-value of 0.3673 and an *F*-value of 0.3673, suggesting that HSRS alone is not a critical factor. In contrast, the FRS was highly significant, with a *p*-value of < 0.0001 and an *F*-value of 873.24, highlighting its substantial impact on Ave_{out}. The interaction term between the HSRS and FRS (AB) was found to be insignificant, with an *F*-value of 0.3074 and a *p*-value of 0.5966, indicating no notable combined effect on Ave_{out} beyond their impacts. Notably, the quadratic term for FRS (B^2) is significant (*p*-value = 0.0171, *F*-value = 9.67), demonstrating a quadratic relationship with Ave_{out}.

For MRT, the model is statistically significant, with an *F*-value of 4.55 and a *p*-value of 0.0363, indicating that the included factors explain a significant portion of the variation in MRT. Similarly, the N_{Re} model is significant, with an *F*-value of 132.66 and a *p*-value of < 0.0001, effectively linking the factors to variations in N_{Re}.

Moreover, the perturbation plots illustrate that MRT and N_{Re} are more sensitive to changes in FRS than HSRS, as evidenced by the steep curves. The statistical significance of the models was further validated by the lack of fit *p*-values. Diagnostic plots, including the Q-Q plot and residual vs. factor plots, indicate that the residuals are normally distributed and randomly scattered, affirming the model's fit. These results underscore that HSR reactors can be finely controlled by adjusting the HSRS and FRS, which enhances reactor performance and biomass conversion efficiency. Accurate prediction of these parameters is crucial for optimizing mixing rates, ensuring uniform heat distribution, and maintaining consistent biomass feed rates. This study offers valuable insights for improving HSR performance and developing more efficient and sustainable biomass conversion processes.

5. Conclusion

This study presents a novel and systematic investigation into the hydrodynamics of an HSIR fluidized bed reactor under continuous flow conditions, utilizing cold test modeling. For the first time, RSM was employed to develop predictive models for key performance indicators, MRT, Ave_{out}, and N_{Re}, offering a powerful framework for optimizing HSIR reactor operations.

Our findings reveal that Feeder Rotation Speed (FRS) exerts a dominant influence on all three parameters, with statistically significant effects confirmed via ANOVA and supported by perturbation analysis and residual diagnostics. Conversely, Helical Screw Rotation Speed (HSRS) showed a limited direct effect, particularly on Ave_{out}, but still played a supporting role in modifying flow behavior and turbulence levels. The identification of a quadratic relationship between FRS and Ave_{out} underscores the need for precise control strategies, as non-linear effects play a critical role in process efficiency. The desirability-based optimization approach demonstrated that optimal combinations of FRS and HSRS can yield superior outcomes, balancing flow rate, residence time, and flow regime to suit operational objectives. The high predictive strength of the RSM models (reflected by high R^2 and adequate precision values) ensures their reliability for guiding future reactor designs and real-time control applications.

The novelty of this work lies not only in its focus on a rarely studied reactor configuration (HSIR) but also in its integrative optimization strategy. By combining detailed RTD analysis, robust experimental design, and desirability-driven multi-objective optimization, this research delivers a comprehensive methodology for enhancing continuous biomass conversion systems. It offers foundational insights into flow behavior, mass transfer, and reactor responsiveness, parameters critical to scaling up thermochemical processes such as pyrolysis, torrefaction, and combustion. Ultimately, this study provides both practical optimization tools and a theoretical understanding of the improved design and operation of HSIR systems. It contributes significantly to the broader goal of developing energy-efficient and sustainable biomass processing technologies, paving the way for future innovations in reactor engineering and renewable energy systems.

Acknowledgments

This work was financially supported by the Ministry of Higher Education Malaysia via the Fundamental Research Grant Scheme DP KPT (FRGS/1/2022/TK05/UM/02/31), and the University of Malaya RU grants GPF025A-2023.

Author contribution statement

Arash Javanmard: Conceptualization; Data collection and Curation; Methodology; Investigation; Formal analysis; Validation; Visualization; Writing original draft; Reviewing, and Editing.

Prof. Dr. Wan Mohd Ashri Wan Daud: Supervision; Funding acquisition; Project administration; Validation.

Dr. Fathiah Mohamed Zuki: supervision; resources; writing, reviewing, and editing.

Dr. Muhamad Fazly Abdul Patah: Supervision; Funding acquisition; Project administration; validation.

All authors reviewed the results and approved the final version of the manuscript.

Availability of data

The data used is presented in tables and figures within the article. The corresponding author will supply any additional or related information upon request.

Conflict of interest

The authors declare no competing financial interest.

Reference

Abdulyekeen, K. A., Daud, W. M. A. W., & Patah, M. F. A. (2024). Valorization of organic municipal solid waste to enhanced solid biofuel: torrefaction kinetics, torrefied solid fuel performance, and fuel properties. *Energy Sources, Part A: Recovery, Utilization, and Environmental Effects, 46*(1), 348-361. https://doi.org/10.1080/15567036.2023.2283616

Abdulyekeen, K. A., Daud, W. M. A. W., Patah, M. F. A., & Abnisa, F. (2022). Torrefaction of organic municipal solid waste to high calorific value solid fuel using batch reactor with helical screw induced rotation. *Bioresource Technology, 363*, 127974. https://doi.org/10.1016/j.biortech.2022.127974

Adeniyi, A. G., Iwuozor, K. O., Emenike, E. C., Ajala, O. J., Ogunniyi, S., & Muritala, K. B. (2024). Thermochemical co-conversion of biomass-plastic waste to biochar: A review. *Green Chemical Engineering, 5*(1), 31-49.

Alauddin, Z. A. B. Z., Lahijani, P., Mohammadi, M., & Mohamed, A. R. (2010). Gasification of lignocellulosic biomass in fluidized beds for renewable energy development: A review. *Renewable and Sustainable Energy Reviews, 14*(9), 2852-2862.

Alonso, E., Gallo, A., Roldán, M., Pérez-Rábago, C., & Fuentealba, E. (2017). Use of rotary kilns for solar thermal applications: Review of developed studies and analysis of their potential. *Solar Energy, 144*, 90-104.

Alsarraf, J., Alnaqi, A. A., & Al-Rashed, A. A. (2025). Geometric optimization of a turbulator in nanofluid flow around a bundle of nuclear reactor fuel rods using the response surface methodology. *Annals of Nuclear Energy, 220*, 111504.

Bhalode, P., Tian, H., Gupta, S., Razavi, S. M., Roman-Ospino, A., Talebian, S., Singh, R., Scicolone, J. V., Muzzio, F. J., & Ierapetritou, M. (2021). Using residence time distribution in pharmaceutical solid dose manufacturing–A critical review. *International Journal of Pharmaceutics, 610*, 121248.

Cai, Q., Lee, B., Ong, S., & Hu, J. (2021). Fluidized-bed Fenton technologies for recalcitrant industrial wastewater treatment–Recent advances, challenges and perspective. *Water Research, 190*, 116692.

Chen, Z., Chen, H., Xu, Y., Hu, M., Hu, Z., Wang, J., & Pan, Z. (2023). Reactor for biomass conversion and waste treatment in supercritical water: A review. *Renewable and Sustainable Energy Reviews, 171*, 113031.

Cherkasov, N., Adams, S. J., Bainbridge, E. G., & Thornton, J. A. (2023). Continuous stirred tank reactors in fine chemical synthesis for efficient mixing, solids-handling, and rapid scale-up. *Reaction Chemistry & Engineering, 8*(2), 266-277.

Cremers, M., Koppejan, J., Middelkamp, J., Witkamp, J., Sokhansanj, S., Melin, S., & Madrali, S. (2015). Status overview of torrefaction technologies: a review of the commercialisation status of biomass torrefaction. *IEA Bioenergy*, 1-52.

Dianyu, E., Tan, C., Li, J., Shi, G., Liu, Y., Liu, S., Yi, L., Zhou, Z., & Cui, J. (2024). Balancing ventilation performance and energy conservation: An integrated multi-objective optimization and preference-based decision-making model for optimizing impinging jet ventilation. *Applied Thermal Engineering, 245*, 122862.

Ding, C., Lei, H., Chen, S., Zhang, H., Zhao, Y., & Zou, Z. (2022). Challenge of residence time distribution curve in tundish for continuous casting of steel. *Steel Research International, 93*(10), 2200187.

Goyal, H., Chen, T.-Y., Chen, W., & Vlachos, D. G. (2022). A review of microwave-assisted process intensified multiphase reactors. *Chemical Engineering Journal, 430*, 133183.

Hanchate, N., Ramani, S., Mathpati, C., & Dalvi, V. H. (2021). Biomass gasification using dual fluidized bed gasification systems: A review. *Journal of Cleaner Production, 280*, 123148.

Harkare, V., Mangrulkar, R., Thorat, O., & Jain, S. R. (2024). Evolutionary approaches for multi-objective optimization and pareto-optimal solution selection in data analytics. In *Applied multi-objective optimization* (pp. 67-94). Springer.

Huter, M. J., & Strube, J. (2019). Model-based design and process optimization of continuous single pass tangential flow filtration focusing on continuous bioprocessing. *Processes, 7*(6), 317.

Infiesta, L. R., Ferreira, C. R., Trovó, A. G., Borges, V. L., & Carvalho, S. R. (2019). Design of an industrial solid waste processing line to produce refuse-derived fuel. *Journal of Environmental Management, 236*, 715-719.

Javanmard, A., Daud, W. M. A. W., Patah, M. F. A., & Ying, C. Y. (2025). Impact of water-washing pretreatment on key properties of torrefied palm kernel shells: A statistical optimization study. *Industrial Crops and Products, 228*, 120729. https://doi.org/10.1016/j.indcrop.2025.120729

Javanmard, A., Wan Daud, W. M. A., & Patah, M. F. A. (2023). The good, the bad, the advantage of washing pretreatment in reducing slagging and fouling index during the torrefaction process. *Process Safety and Environmental Protection, 176*, 852-866. https://doi.org/10.1016/j.psep.2023.06.065

Javanmard, A., Wan Daud, W. M. A., Patah, M. F. A., Zuki, F. M., Ai, S. P., Azman, D. Q., & Chen, W.-H. (2024). Breaking barriers for a green future: a comprehensive study on pre-treatment techniques for empty fruit bunches in the bio-based economy. *Process Safety and Environmental Protection, 182*, 535-558. https://doi.org/10.1016/j.psep.2023.11.053

Javanmard, A., Zuki, F. M., Patah, M. F. A., & Daud, W. M. A. W. (2024). Revolutionizing microbial fuel cells: Biochar's energy conversion odyssey. *Process Safety and Environmental Protection, 187*, 26-58. https://doi.org/10.1016/j.psep.2024.04.066

Javanmard, A., Zuki, F. M., Patah, M. F. A., & Wan Daud, W. M. A. (2025). Transforming biowaste to bioenergy: the role of catalysts in advancing thermochemical torrefaction. *Process Safety and Environmental Protection*, 106779. https://doi.org/10.1016/j.psep.2025.106779

Khodaei, H., Al-Abdeli, Y. M., Guzzomi, F., & Yeoh, G. H. (2015). An overview of processes and considerations in the modelling of fixed-bed biomass combustion. *Energy, 88*, 946-972.

Korba, D., Huang, W., Randhir, K., Petrasch, J., Klausner, J., AuYeung, N., & Li, L. (2022). A continuum model for heat and mass transfer in moving-bed reactors for thermochemical energy storage. *Applied Energy, 313*, 118842.

Lacombe, E., Grateau, M., Marchand, M., Melkior, T., & Dupont, C. (2024). Torrefaction of oak and olive stones in a semi-industrial multiple hearth furnace: Products yields and composition. *Biomass and Bioenergy, 181*, 107057.

Lambrinidis, G., & Tsantili-Kakoulidou, A. (2021). Multi-objective optimization methods in novel drug design. *Expert Opinion on Drug Discovery, 16*(6), 647-658.

Lewandowski, W. M., Ryms, M., & Kosakowski, W. (2020). Thermal biomass conversion: A review. *Processes, 8*(5), 516.

Li, J. (2016). Assessing spatial predictive models in the environmental sciences: Accuracy measures, data variation and variance explained. *Environmental Modelling & Software, 80*, 1-8.

Moser, K., Wopienka, E., Pfeifer, C., Schwarz, M., Sedlmayer, I., & Haslinger, W. (2023). Screw reactors and rotary kilns in biochar production–A comparative review. *Journal of Analytical and Applied Pyrolysis,* 106112.

Motta, I. L., Miranda, N. T., Maciel Filho, R., & Maciel, M. R. W. (2018). Biomass gasification in fluidized beds: A review of biomass moisture content and operating pressure effects. *Renewable and Sustainable Energy Reviews, 94*, 998-1023.

Nachenius, R., van de Wardt, T., Ronsse, F., & Prins, W. (2015). Torrefaction of pine in a bench-scale screw conveyor reactor. *Biomass and Bioenergy, 79*, 96-104.

Ofélia de Queiroz, F. A., Morte, I. B. B., Borges, C. L., Morgado, C. R., & de Medeiros, J. L. (2024). Beyond clean and affordable transition pathways: A review of issues and strategies to sustainable energy supply. *International Journal of Electrical Power & Energy Systems, 155*, 109544.

Qureshi, K. M., Abnisa, F., & Wan Daud, W. M. A. (2019). Novel helical screw-fluidized bed reactor for bio-oil production in slow-pyrolysis mode: A preliminary study. *Journal of Analytical and Applied Pyrolysis, 142*, 104605. https://doi.org/10.1016/j.jaap.2019.04.021

Qureshi, K. M., Kay Lup, A. N., Khan, S., Abnisa, F., & Wan Daud, W. M. A. (2021). Optimization of palm shell pyrolysis parameters in helical screw fluidized bed reactor: Effect of particle size, pyrolysis time and vapor residence time. *Cleaner Engineering and Technology, 4*, 100174. https://doi.org/10.1016/j.clet.2021.100174

Qureshi, K. M., Lup, A. N. K., Khan, S., Abnisa, F., & Daud, W. M. A. W. (2021). Effect of temperature and feed rate on pyrolysis oil produced via helical screw fluidized bed reactor. *Korean Journal of Chemical Engineering, 38*, 1797-1809.

Qureshi, M. S., Oasmaa, A., Pihkola, H., Deviatkin, I., Tenhunen, A., Mannila, J., Minkkinen, H., Pohjakallio, M., & Laine-Ylijoki, J. (2020). Pyrolysis of plastic waste: Opportunities and challenges. *Journal of Analytical and Applied Pyrolysis, 152*, 104804.

Reji, M., & Kumar, R. (2022). Response surface methodology (RSM): An overview to analyze multivariate data. *Indian Journal of Microbiology Research, 9*, 241-248.

Rodrigues, A. E. (2021). Residence time distribution (RTD) revisited. *Chemical Engineering Science, 230*, 116188.

Sadrossadat, E., Basarir, H., Karrech, A., & Elchalakani, M. (2022). Multi-objective mixture design and optimisation of steel fiber reinforced UHPC using machine learning algorithms and metaheuristics. *Engineering with Computers, 38*(Suppl 3), 2569-2582.

Seurin, P., & Shirvan, K. (2024). Multi-objective reinforcement learning-based approach for pressurized water reactor optimization. *Annals of Nuclear Energy, 205*, 110582.

Sharma, A., Kodgire, P., & Kachhwaha, S. S. (2019). Biodiesel production from waste cotton-seed cooking oil using microwave-assisted transesterification: Optimization and kinetic modeling. *Renewable and Sustainable Energy*

Reviews, 116, 109394.
Siwal, S. S., Sheoran, K., Saini, A. K., Vo, D.-V. N., Wang, Q., & Thakur, V. K. (2022). Advanced thermochemical conversion technologies used for energy generation: Advancement and prospects. *Fuel, 321*, 124107.
Soponpongpipat, N., Nanetoe, S., & Comsawang, P. (2020). Thermal and torrefaction characteristics of a small-scale rotating drum reactor. *Processes, 8*(4), 489.
Soria-Verdugo, A., Cano-Pleite, E., Passalacqua, A., & Fox, R. O. (2023). Effect of particle shape on biomass pyrolysis in a bubbling fluidized bed. *Fuel, 339*, 127365.
Stegehake, C., Riese, J., & Grünewald, M. (2019). Modeling and validating fixed-bed reactors: a state-of-the-art review. *ChemBioEng Reviews, 6*(2), 28-44.
Tumuluru, J. S., Ghiasi, B., Soelberg, N. R., & Sokhansanj, S. (2021). Biomass torrefaction process, product properties, reactor types, and moving bed reactor design concepts. *Frontiers in Energy Research, 9*, 728140.
Ünsaç, A., Okutan, H. C., & Karatepe, N. (2024). Low tar yield and high energy conversion efficiency in a continuous pyrolysis reactor with modified ribbon screw conveyor. *International Journal of Hydrogen Energy, 53*, 1332-1343.
Vaithyanathan, V. K., Goyette, B., & Rajagopal, R. (2023). A critical review of the transformation of biomass into commodity chemicals: Prominence of pretreatments. *Environmental Challenges*, 100700.
Veza, I., Spraggon, M., Fattah, I. M. R., & Idris, M. (2023). Response surface methodology (RSM) for optimizing engine performance and emissions fueled with biofuel: Review of RSM for sustainability energy transition. *Results in Engineering, 18*, 101213. https://doi.org/10.1016/j.rineng.2023.101213
Wang, B., Xu, F., Wang, X., Li, J., Song, Y., Qiao, Y., & Tian, Y. (2022). Comparative study on pyrolysis and gasification within CO_2 atmosphere of typical forestry biomass in Northeast Asia: Thermal behavior and kinetic analysis. *Fuel, 324*, 124540.
Weremfo, A., Abassah-Oppong, S., Adulley, F., Dabie, K., & Seidu-Larry, S. (2023). Response surface methodology as a tool to optimize the extraction of bioactive compounds from plant sources. *Journal of the Science of Food and Agriculture, 103*(1), 26-36.
Wojewódka, P., Aranowski, R., & Jungnickel, C. (2019). Residence time distribution in rapid multiphase reactors. *Journal of Industrial and Engineering Chemistry, 69*, 370-378. https://doi.org/10.1016/j.jiec.2018.09.037
Wu, M., Jurtz, N., Walle, A., & Kraume, M. (2022). Evaluation and application of efficient CFD-based methods for the multi-objective optimization of stirred tanks. *Chemical Engineering Science, 263*, 118109.